12,03

Space-charge-limited carrier localization in InGaN/GaN quantum wells

© N.I. Bochkareva, Y.G. Shreter

Ioffe Institute,
St. Petersburg, Russia

E-mail: n.bochkareva@mail.ioffe.ru

Received November 12, 2021
Revised November 12, 2021
Accepted November 13, 2021

The mechanism of carrier tunneling through the potential walls of InGaN/GaN quantum well in the $p-n$-structures is studied by means of the deep center tunneling spectroscopy. A number of humps on the current and photocurrent tunneling spectra, as well as on the forward bias dependences of the intensity and the peak energy of photoluminescence band from the quantum well are detected. These findings allow us to propose a model of carrier localization in the quantum well that permit to relate the tunneling transparency of the potential walls of the QW to the space-charge of deep-level centers in the quantum well barriers and its changes under optical excitation and forward biasing of $p-n$-structure.

Keywords: gallium nitride, quantum well, photoluminescence, deep center tunneling spectroscopy, impurity color centers.

DOI: 10.21883/PSS.2022.03.53193.241

1. Introduction

In structures with InGaN/GaN quantum wells, which are the basic element of solid-state light sources [1,2], the high quantum efficiency of radiative recombination is achieved despite the high density of structural lattice defects (dislocations, stacking faults), as well as point defects and their complexes which form the deeper distribution of localized states in the GaN band-gap ($E_{g,\mathrm{GaN}} = 3.42\,\mathrm{eV}$ at $300\,\mathrm{K}$) than in amorphous Si [3]. Gallium nitride made it possible not only to change the established notion that a high density of dislocations excludes the acceptable performance of optoelectronic devices [1], but also to demonstrate the possibility of realizing quantum efficiency in a material with „dirty“ band-gap, reaching 86% [2].

Already early experimental studies showed the dominant role of defects in the tunneling mechanism of current flow through potential barriers in light-emitting and photovoltaic nanostructures, as well as in the gates of field-effect transistors based on GaN [4–6]. However, the mechanism of tunneling involving defects and its role in problems critical for the development of solid-state illumination, including the problems of decreasing the quantum efficiency in high-power optoelectronic devices and increasing their durability, have not yet been studied enough.

Theoretically, trap-assisted tunneling (hopping) through the barrier created by the band-gap is considered based on the approaches used earlier to describe tunneling leakage currents in dielectrics and excess current in tunneling diodes and non-ideal heterojunctions, which assumed tunneling through discrete centers [7], the impurity band [8], or through centers with a uniform energy distribution [9]. However, GaN epitaxial layers and InGaN/GaN quantum wells are characterized by deep tails of localized states, which are inherent in disordered and partially disordered media, in which the high density of states allows carriers to tunnel by hops between local centers.

In that way, the broad emission spectra of InGaN/GaN quantum wells are well described in the model of exciton thermalization adopted for disordered solid solutions [10] due to tunnel junctions with the participation of phonons between states of exponential tails, which are associated with compositional fluctuations of the band-gap of the solid solution $\mathrm{In}_x\mathrm{Ga}_{1-x}\mathrm{N}$ [11]. In epitaxial GaN layers, hopping conduction through local impurity centers makes a significant contribution to electron transport even at room temperature and dominates with temperature decreasing [12].

The continuous energy spectrum of defects in the band-gap of GaN has features associated with impurity bands of deep centers, including oxygen- and hydrogen-substituted vacancies. Point defect complexes cause broad bands of intracenter absorption and photoluminescence (PL) in the visible region of the spectrum (color centers), as well as in the near IR and near UV regions (i.e., IR and UV color centers) [11,13,14]. The small Stokes shift between the wavelengths of excitation and emission of intracenter PL in GaN indicates that excited carriers are thermalized due to tunnel junctions involving phonons between localization centers. The slow kinetics of PL decay [11] reflects the exponential decay of the rate of tunneling to deeper states with lower density. Kinetics characterized by a stretched exponential curve was also observed for transient forward currents in $p-n$-structures with InGaN/GaN quantum wells [15]. It should be expected that the rate of tunneling charge transfer through

the barrier during electric injection is limited by the frequency of hops near the quantum well, in the layer with the lowest density of local centers along the tunneling length. This makes it possible to use the Esaki tunneling spectroscopy method to study the spectrum of defects, which provides information on the energy levels in solid states: in thin layers of insulators and narrow semiconductor $p-n$-junctions [7]. The experimental current-voltage characteristics of a forward-biased $p-n$-junction are analyzed in this method under the assumption that the tunneling rate is determined by the density of empty final states at the junction boundary. At the same time, in the case of the high density of local centers, the probability of tunnel junction through the triangular potential barrier in a strong electric field, calculated by Keldysh [16], can significantly decrease as a result of recharging of local centers and the decrease in the space-charge density and field strength.

In this work, we present experimental data on the mechanism of tunneling current and luminescence in $p-n$-structures with single InGaN/GaN quantum wells. The dependences of the tunneling current on forward bias reveal interesting features. The maxima of the tunneling current on the „dark" $I-V$ curves correspond to the minimums of the tunneling current upon optical excitation, as well as the humps in the dependences of the intensity and spectral shift of the PL band from the quantum well on the bias. These observations allow us to propose the model of carrier localization in the quantum well that relates the tunneling permeability of the potential walls of the well to the space charge density of deep centers and its change upon optical excitation and forward bias of the $p-n$-structure.

2. Experiment and experimental results

For the study were selected: two types of light-emitting $p-n$-structures with the single InGaN/GaN quantum well 30 Å thick, emitting in the blue region of the spectrum with a peak radiation energy $h\nu_p = 2.65$ eV ($\nu_p = 465$ nm) at rated current $I = 20$ mA (structure area 10^{-3} cm^2). The structures differ in the magnitude of the internal quantum efficiency of electroluminescence (EL), which in the structures designated as A and B, is 60 and 40%, respectively, and in the level of tunneling leakage currents, which are ~ 1 nA and 3 μA, respectively, at a bias $V_{th} = 2.2$ eV required to detect the threshold EL intensity. Structure details are shown in [17,15]. According to measurements of the capacitance-voltage characteristics showed, n-and p-regions in nanostructures A are heavily doped ($> 3 \cdot 10^{18}$ cm^{-3}), but in the n-GaN layer there is a weakly doped ($7 \cdot 10^{16}$ cm^{-3}) area with the width of ~ 120 ,nm bordering on the quantum well. In nanostructures B, the n-region is doped much more heavily (10^{18} cm^{-3}) than the p-region ($\sim 2 \cdot 10^{17}$ cm^{-3}).

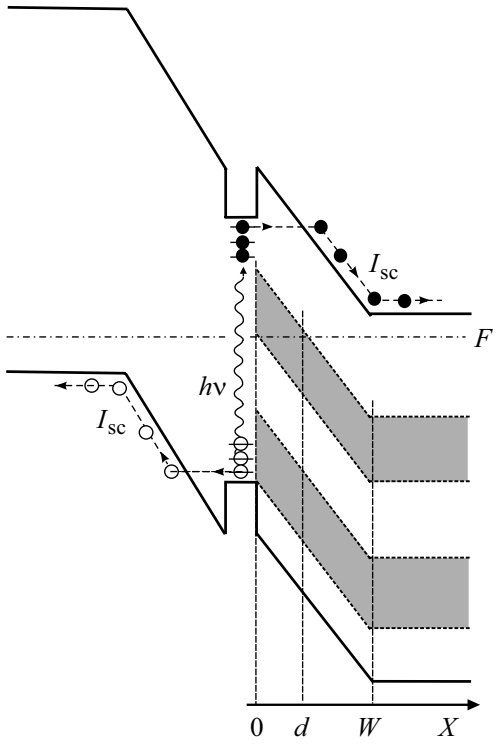

Figure 1. Energy bands diagram of $p-n$-structures with InGaN/GaN quantum well.

Measurements of current-voltage characteristics were carried out using the current and voltage source-measuring device by Keithley 238. Subbandgap optical excitation was carried out with the light of a tungsten incandescent lamp. Photoluminescence was excited by a He−Cd laser with a power of 20 mW at a wavelength of 325 nm ($h\nu = 3.81$ eV). The PL spectra were recorded on AvaSpec-2048 spectrometer.

Under subbandgap excitation of $p-n$-structures with an InGaN/GaN quantum well with photon energy $E_{g,\mathrm{GaN}} > h\nu > h\nu_p$, optically generated carriers tunnel out of the quantum well and, separating in the $p-n$-junction field, generate the photocurrent (Fig. 1) [11,18].

Dependences of current on forward bias V in electron-volts ($V \equiv F_n - Fp$ — difference between electronic and hole Fermi levels) for $p-n$-structures A and B measured in the „dark", i.e. in the absence of optical excitation, and in the case of subbandgap optical excitation, are shown in Fig. 2. In Fig. 3, *a, b* the dependences of the dark current I on the forward bias are shown on the semilogarithmic scale (curves *1*).

In structure A, the forward dark current first sharply increases to the maximum value $I_p = 0.06$ nA at a bias $V_p = 0.31$ eV, then, after slight drop in the current in the region with a negative differential conductivity, one more relative maximum is observed (Fig. 3, *a*, curve *1*). With a further increase in the bias, three „humps" of the tunneling current are observed, and the current between the humps increases monotonically with increasing bias. At the bias of

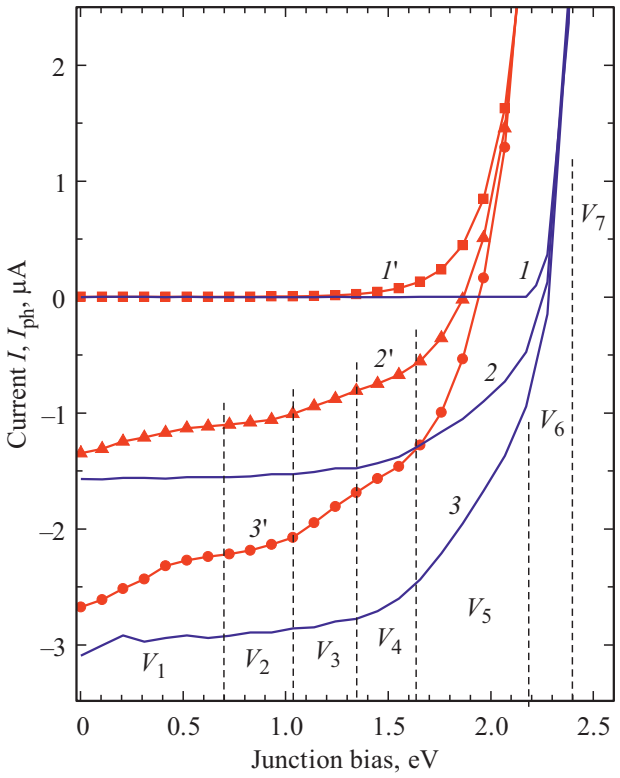

Figure 2. Current dependencies on forward bias for structures A ($1-3$) and B ($1'-3'$) measured in „dark" ($1, 1'$) and under subbandgap optical excitation ($2, 3, 2', 3'$). Excitation power, mW/cm^2: $2, 2'$ — 50, $3, 3'$ — 100. The dashed lines mark the intervals of the V_1-V_7 bias's indicated in Fig. 3, *a*.

$V = 1.65$ eV, the excess tunneling current begins to grow sharply and exceeds the peak current in magnitude I_p. The sharpest stepwise growth of the tunneling current is observed near the threshold bias $V_{th} = 2.2$ eV. In structure B, near zero bias, the dark current is equal to the current in structure A, but with increasing bias, the current increases approximately according to an exponential law and, near the threshold bias, exceeds the dark current in structure A by more than three orders of magnitude (Fig. 3, *b*, curve *1*).

Please note that the dark $I-V$-characteristic of the A structure has much in common with the $I-V$-characteristics of narrow tunnel junctions, in which both sides of the junction are doped up to degeneration. The maximum tunneling current I_p at the bias $V_p = 0.31$ eV resembles a similar maximum in tunnel junctions due to interband tunneling. The maximum at the decay of the tunneling current peak was also observed in tunnel junctions, where it was associated with the excess tunneling current through deep centers of defects [19], as well as current humps in the valley of $I-V$-characteristics. In structure A, the amplitude of the tunneling current maximum is very small, but the ratio of the peak current to the valley current, which is one of the indicators of the quality of the tunnel junction, is high: $I_p/I_v = 10$.

It can be seen from Fig. 2 that in $p-n$-structures the rule of additivity of an ideal photodiode or solar cell, according to which the photocurrent $I_{ph} = I_{sc} + I$ is equal to the sum of short-circuit photocurrent I_{sc}, flowing in the opposite direction ($I_{sc} < 0$) and independent of voltage, and forward current ($I > 0$), independent of illumination. Comparison of the $I_{ph}-V$ and $I-V$ curves shows that the photocurrent decreases with increasing bias faster than the forward dark current increases.

The nature of the change in the photocurrent with increasing forward bias is illustrated in Fig. 3, *a, b*, where the dependences $I_{opt}(V) = I_{ph} - I_{sc}$ are shown on a semilogarithmic scale for structure B at different levels of excitation (Fig. 3, *b*, curves *2–4*) and for structure A at a high level of excitation (Fig. 3, *a*, curve *4*). At lower excitation levels, the photocurrent in the structure A increases to $I_{\max}$ as the bias increases to ~ 0.4 eV, and the nature of the change in the photocurrent under these conditions is illustrated by the curves $I_{opt}(V) = I_{ph} - I_{\max}$ (Fig. 3, *a*, curves *2, 3*).

Subbandgap optical excitation leads to the strong increase in the tunneling current, and in the structure A in the area of the humps of the dark tunneling current on the $I-V$ curves, dips in the light tunneling current I_{opt} are observed (Fig. 3, *a*, curves *2, 3*). With the increase in the excitation level on the $\lg I_{opt}(V)$ curves of the structure B, the steps in the region of the same bias's as the dark current humps in the structure A become more and more distinguishable (Fig. 3, *b*, curve *4* and Fig. 2, curve *3'*).

Under interband excitation by laser radiation ($h\nu = 3.81$ eV), photoluminescence from the quantum well and photocurrent are observed in the structures. Figure 4 shows the dependences on the forward bias of the dark current $I(V)$ and the dependences $I_{opt}(V) = I_{ph}(V) - I_{sc}$, which characterize the decrease in the photocurrent with increasing bias at interband excitation, as well as the shift dependence of the photoluminescence intensity $I_{\mathrm{PL}}(V)$ and the peak photoluminescence energy $h\nu_{\mathrm{PL}}(V)$ for structure B.

As can be seen from Fig. 4, the distinguishable humps on the $I_{opt}(V)$ curves under interband excitation (curve *2*) are observed in the region of the same bias's as under subbandgap excitation (Fig. 2, curve *3'* and Fig. 3, *b*, curve *4*). It can also be seen from Fig. 4 that the intensity and red shift of the peak photoluminescence energy from the quantum well increase with increasing forward bias faster in those bias intervals in which the photocurrent decreases faster.

3. Discussion of results

Tunneling permeability and tunneling conductance of the potential barrier. In its simplest form, the tunneling permeability of a potential barrier with height φ, which determines the probability of a charge carrier tunneling from a busy initial state with energy E to an empty final state with

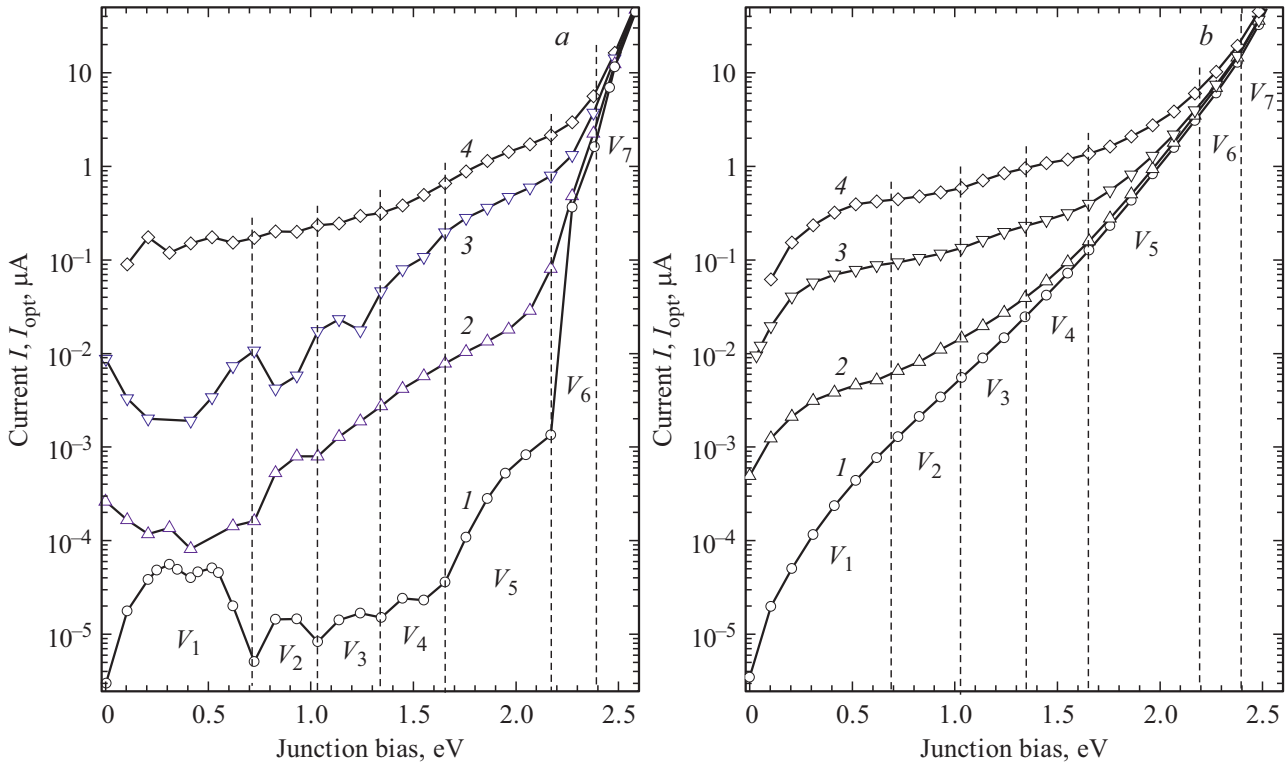

Figure 3. Current dependencies on forward bias for structures A (*a*) and B (*b*) measured in „dark" (*1*) and under subbandgap optical excitation (*2–4*). Excitation power, mW/cm^2: *2* — 1, *3* — 50, *4* — 100. The dashed lines mark the intervals of V_1–V_7 bias's, where humps and steps are observed on the curve *1* (*a*).

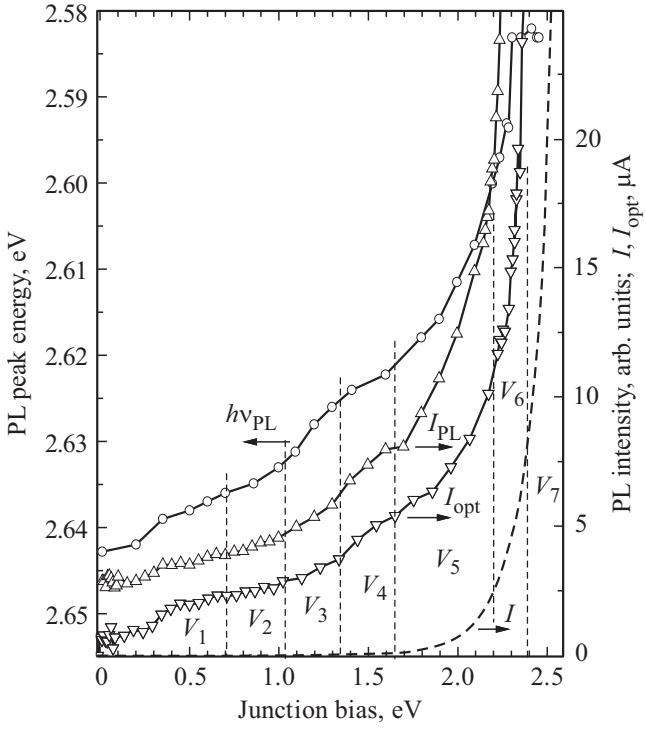

Figure 4. Dependences of forward current I_{opt}, photoluminescence intensity I_{PL}, and peak photoluminescence energy $h\nu_{PL}$ under laser excitation and forward current in the absence of excitation I from forward bias for structure B. The dashed lines mark the same bias intervals V_1–V_7 as in Fig. 3, *a*. $T = 300$ K.

the same energy, has the form [16]:

$$D = \exp\left(-\frac{\pi\delta}{2\sqrt{2\hbar}}\sqrt{2m^*\varphi}\right), \qquad (1)$$

where $\delta = \varphi/F = (\varepsilon/q^2N_t)^{1/2}$ — barrier width, F — electric field strength, N_t — density of ionized impurities, q — electron charge, ε — permittivity, m^* — reduced effective mass of electron and hole.

The differential tunneling conductivity of the g_{tun} barrier is proportional to the product of three functions: the densities of occupied initial $\rho_s(E_t)$ and empty final $\rho_f(E_t)$ states on the isoenergetic transport level E_t and tunneling permeability $D(E_t)$ [9]:

$$g_{tun} \equiv dI/dE_t = AD(E_t)\rho_s(E_t)\rho_f(E_t), \qquad (2)$$

here, A is a constant value.

Esaki deep center tunneling spectroscopy [7] is based on the assumption that the barrier width in the p–n-junction is determined by the concentration of the main dope additive. The barrier height decreases with forward bias: $\varphi = \varphi_0 - V$ (φ_0/q — contact potential difference), and the permeability increases exponentially with increasing bias: $D \propto \exp(C_1V)$, where C_1 is a constant. The flow of majority carriers from the allowed zone tunnels through the barrier on the less doped side of the junction to the boundary of the p–n-junction, where the majority carriers recombine with

minority carriers diffusing from the opposite side of the junction. As a result of the Boltzmann energy distribution of free carriers, the main flux tunnels near the Fermi quasi-level. It is assumed that the excess tunneling current at a given bias increases linearly with an increase in the density of empty final states with energy E_t at the junction boundary $\rho_f(E_t)$ (E_t counts down from the Fermi level at the junction boundary). The maxima of the density of states $\rho_f(E_t)$ appear as tunneling current humps on the $I-V$-characteristics.

In materials with a high density of localized states, the tunneling of carriers through a potential barrier can be considered based on the model of dispersive transport [20,21]: carriers at the edge of the neutral region make a tunnel junction to the nearest local center, and reach more distant ones by hopping along centers at the tunnel transport layer E_t. The hopping frequency and local tunneling conductance decrease exponentially with increasing distance between local centers at the E_t level [21].

The similarity of the shape of $I-V$-characteristics of the nanostructure A (Fig. 3, *a*, curve *1*) and tunnel junctions noted above suggests that due to the high density of defects (taking into account their possible sink to threading dislocations and grain boundaries), at the periphery of the space charge region (SCR), the distance between local centers (in a layer of thickness $w-d$ in Fig. 1) is small enough to ensure its high tunneling conductivity. The main contribution to the tunneling resistance of the barrier $r = 1/g_{tun}$ comes from the tunneling resistance of the near-boundary layer (layer of thickness d in Fig. 1) with the highest localization energy of centers at the tunneling transport layer E_t. The forward bias increment is distributed between the *n*-and *p*-barriers in proportion to the tunneling resistances of their boundary layers r_n and r_p ($r_n + r_p = r$).

The tunnel-recombination current flows in a $p-n$-structure with the quantum well: electrons and holes tunnel through the barriers and recombine in the space charge region. The continuity of the current is ensured by the equality of the tunneling flows of electrons and holes. Color centers, like molecular complexes, form impurity bands in the upper and lower halves of the band-gap. The current maximum or step occurs at such a forward bias $V \equiv F_n - F_p$, when the Fermi electronic level F_n at the boundary between the quantum well and the *n*-region of the junction will be at the level of the maximum density of states of the impurity band of color centers in the upper half of the band-gap, and the hole Fermi level F_p in the *p*-region — at the level of the maximum density of states of the impurity band of these centers in the lower half of the band-gap. In the case of $r_n \approx r_p$, the forward bias increment is equally distributed between the *n*-and *p*-barriers, and the charge carriers recombine at the junction boundary. In the case of strong asymmetry of the tunneling resistances, the bias increment decreases mainly at the barrier with a high tunneling resistance $r_{\max}$, and the carriers recombine predominantly in the SCR of this barrier.

Analysis of the shape of the $I-V$-characteristics (Figs. 2 and 3) also leads to the conclusion that the space charge density of ionized impurity centers is not negligible compared to the density of the main dopant, and their space charge has a significant effect on the tunneling permeability of the boundary layers, controlling the tunneling flows in the $p-n$-structure.

Tunneling spectroscopy of deep levels of defects. Humps and steps in the tunneling spectrum of the dark current $I(V)$ of structure A (Fig. 3, *a*, curve *1*) in the V_i bias intervals ($i = 1, \ldots, 7$) reflect the presence in the band-gap of GaN of several Gaussian impurity bands $\rho_i(E)$ with maxima of the density of states at $E = E_{0i}$ superimposed on a continuous background of impurity states of the Urbach tail $\rho_U(E)$, which propagates, exponentially decreasing, deep into the band-gap.

As the forward bias increases, the transport level E_t in the barrier with $r_{\max}$ near the heterojunction moves to the edge of the allowed band, according to (2), changes behavior of the tunneling conductivity is most strongly influenced by the change in the product of two functions $\rho_f(E_t)D(E_t)$, where $\rho_f(E_t) = \rho_{if}(E_t) + \rho_{Uf}(E_t)$ — total density of empty final states of the impurity band and the Urbach tail with energy E_t, $D(E_t)$ — tunneling permeability of the boundary layer:

$$g_{tun}(E_t) \propto D\left(\frac{d\rho_{if}}{dE_t} + \frac{d\rho_{Uf}}{dE_t}\right) + (\rho_{if} + \rho_{Uf})\frac{dD}{dE_t}. \quad (3)$$

According to (3), the excess in the density of empty final states $d\rho_f(E_t)/dE_t$ when the level E_t moves leads to the greater increase g_{tun}, the higher the permeability of the barrier. But the simultaneous filling and recharging of the final states of the impurity band $\rho_i(E)$ leads to the decrease in the permeability, up to the change in sign g_{tun}. The recharge of deep states of the exponential tail $\rho U(E_t)$ does not lead to a significant decrease $D(E_t)$, since the total charge of its ionized states Q_U is determined by the density of shallow states.

In structure A, the tunneling current maximum at $V_p = 0.31$ eV is caused by the presence of the Gaussian impurity band $\rho_{1f}(E_t)$. The relative maximum at the bias $V = 0.52$ eV can be associated with the increase in the density of states of the impurity Urbach tail $\rho_{Uf}(E_t)$ at the level E_t. Negative differential conductivity $g_{tun} < 0$ arises as a result of a decrease in the tunneling permeability of the barrier with increasing bias, caused by a decrease in the total space charge of the ionized states of the impurity bands $Q_G(E_t)$ upon recharging of the states $\rho_1(E)$ and $\rho_2(E)$. Successive decrease in the tunneling permeability $D(E_t)$ as the bias increases and the states $\rho_i(E)$ ($i = 2, 3, 4$) are recharged, reduces the height of the current humps in the valley of $I-V$-characteristics. The sharp stepwise growth of the tunneling current in the region of bias's V from 1.65 to 2.5 eV is due to the high density of states $\rho_i(E)$ ($i = 5, 6, 7$).

In structure B, in the region of bias's corresponding to the valley of $I-V$-characteristics in structure A, only a weak depression is observed on the $\lg I(V)$ curve (Fig. 3, *b*, curve *1*), which suggests the dominant contribution to the space charge in the near-boundary layer and its high tunneling permeability of the space charge of the ionized states of the Urbach tail $Q_U > Q_G(E_t)$.

Tunneling photoconductivity of SCR (space-charge region) under subbandgap excitation. Under optical excitation, photoionization of deep centers occurs with localization energy $E_{loc} > E_t$ and charge carriers pass into the allowed band, followed by „pulling" of carriers by the electric field from the SCR. The photoinduced space charge Q_{ph} is added to the space charge generated by thermal excitation $Q_{th} = Q_G(E_t) + Q_U$, which increases the field strength in the boundary layer and its tunneling permeability $D(E_t)$.

In a structure A at the low excitation level (Fig. 2, *a*, curve *2*) near zero bias $Q_{ph}/Q_G(0) \approx 1$. Increase in the $Q_{ph}/Q_G(E_t)$ ratio as the states of the impurity bands are recharged with increasing bias leads to an increase in $D(E_t)$ and g_{tun}, which is sharper at the edges of impurity bands at $E_t < E_{0i}$, when the space charge $Q_G(E_t)$ decreases rapidly, and weaker at $E_t > E_{0i}$ when the decrease in $Q_G(E_t)$ and $\rho_{f,i}(E_t)$ is compensated by the increase in $\rho_{f,U}(E_t)$. Decrease in the conductivity g_{tun} is observed only at low biases, when the ratio $Q_G(E_t)/Q_{ph}$ is still quite high and the contribution from the decrease in the space charge $Q_G(E_t)$ at the level E_t into a decrease in permeability $D(E_t)$.

With the increase in the excitation level $Q_G(0) < Q_{ph}$ and dips in the light current I_{opt} in the region of dark current humps I (curve *3*) are caused by the competing effect charge exchange of impurity band states and growth of $\rho_U(E_t)$. But as the ratio $Q_G(E_t)/Q_{ph}$ decreases, the depth of modulation of the tunneling current by the space charge of the impurity bands decreases with increasing bias, and at a high excitation level (at $Q_G(0) \ll Q_{ph}$, the curve *4*) appears only in weak oscillations of the tunneling current with the bias.

In the structure B $Q_U > Q_G(0)$, and the recharging of impurity band states does not lead to negative differential conductivity, but only limits the current growth, causing $\lg I_{opt}(V)$ at high levels of excitation (Fig. 3, *b*, curve *4*) the appearance of distinguishable steps: current cutoff in the region $E_t > E_{0i}$ at $\rho_{f,i}(E_t) > \rho_{f,U}(E_t)$ and $E_t < E_{0i}$ for $\rho_{f,i}(E_t) < \rho_{f,U}(E_t)$.

Photostimulated tunneling permeability of the quantum well walls. The photoinduced space charge Q_{ph} increases the tunneling permeability of the well walls and leads to a weakening of carrier confinement and weak photoluminescence from the quantum well upon interband optical excitation. Successive filling and recharging of the $\rho_i(E)$ states in the boundary layer with increasing bias is accompanied by the decrease in the space charge density Q_G near the boundary. According to (1), at the given barrier height, the tunneling permeability of the well wall decreases exponentially in inverse proportion to the square root of the space charge density of ionized impurities at the heterointerface: $D \propto \exp(-C_2/N_t^{1/2})$, where C_2 is a constant. The decrease in the tunneling permeability of the well wall leads to an increase in the confinement of optically injected carriers, which manifests itself in an increase in the PL intensity from the quantum well.

The higher the carrier localization energy in the quantum well and, accordingly, the lower the radiation energy, the greater the height of the effective barrier through which the carriers tunnel from the quantum well. For deeply localized carriers responsible for emission in the low-energy wing of the spectrum, the thickness of the potential wall along the tunneling path increases more strongly. As the forward bias increases, the red sub-spectrum of the PL spectrum grows much faster than the blue sub-spectrum, which leads to the red shift in the peak energy of the PL band from the quantum well, which accompanies an increase in the photoluminescence intensity.

Nature of centers responsible for tunneling leakage currents. The results of tunneling spectroscopy of deep centers correlate with the known data of optical measurements in GaN. The threshold shift $V = 2.2$ eV, at which the sharp increase in the tunneling current is observed, corresponds to the peak energy $h\nu_p = 2.2$ eV of the yellow PL band (YL) in GaN [1,22] and threshold energy $h\nu_{th}$ of absorption by YL color centers responsible for yellow PL [23,24]. The increase in the tunneling current at the bias $V = 2.4$ eV corresponds to the peak energy $h\nu_p = 2.4$ eV of the green PL band (GL) in GaN [22]. The region of shifts V from 1.65 to 2.2 eV corresponds to the spectral region of absorption by RL color centers responsible for the red PL band (RL) ($h\nu_p = 1.85$ eV) and its impurity Urbach tail extending into the IR region up to $h\nu = 1.65$ eV [1,25]. The number of current humps in the region of bias's 0.7–1.65 eV with approximately equal energy intervals between them presumably reflects a series of bands in the electronic-vibrational structure of the oxygen-containing defect. Current humps with maxima at $V \approx 1.25$ and 1.45 eV correspond to a broad optical absorption band with a maximum at $h\nu = 1.22$ eV, which dominates in GaN by volume [13,23]. The current hump with the maximum at $V \approx 0.8$ eV corresponds to the IR photoluminescence band in the region $h\nu$ from 0.7 to 1 eV with maxima in the vicinity of 0.9 and 0.8 eV [26] and the threshold energy of optical absorption in GaN $h\nu_{th} = 0.78$ eV [27].

Tunneling currents flowing at small forward biases „under" the quantum well reduce the efficiency of electroluminescence at low injection levels. As can be seen from Fig. 5, which shows the temperature dependences of the quantum efficiency $\eta = I_{\mathrm{EL}}/I$ (I_{EL} — EL intensity) at a current $I = 3\,\mu$A, structures A and B differ significantly not only in the value of the efficiency at room temperature, but also in its temperature dependence, which characterizes the temperature behavior of the tunneling leakage current. The efficiency of structure A rapidly increases upon cooling from 300 to ~ 200 K, and only weakly increases upon cooling below ~ 160 K. In structure B, the efficiency is

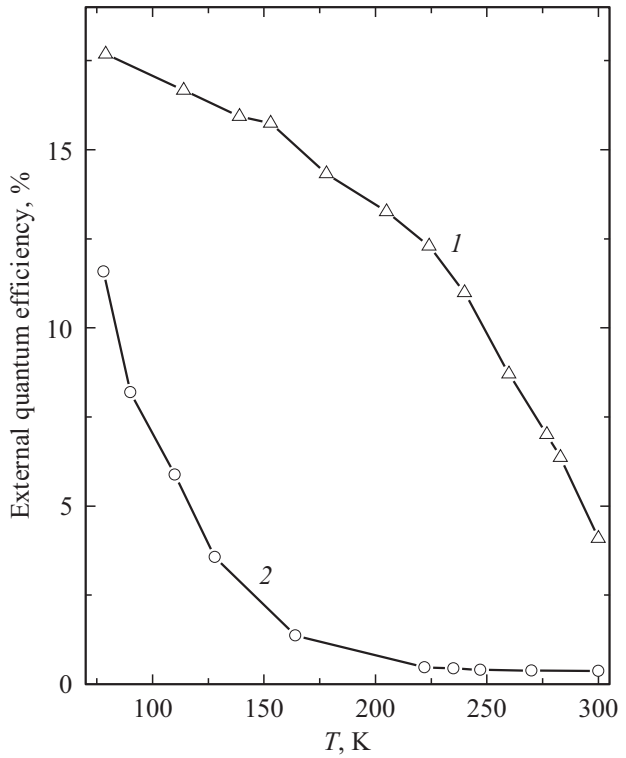

Figure 5. Temperature dependences of quantum efficiency of electroluminescence $\eta = I_{EL}/I$ of structures A (*1*) and B (*2*) at $I = 3\,\nu$A.

almost constant in the temperature range of 300−200 K and rapidly increases upon cooling from ∼ 160 to 80 K.

In the structure A with the heavily doped *p*-region ($> 3 \cdot 10^{18}\,\mathrm{cm}^{-3}$), the nature of the tunneling current spectrum $I(V)$ in the region of bias's 2.2−2.5 eV corresponds to the PL spectrum $I_{PL}(h\nu)$ of *p*-GaN layers with hole concentration $\sim 10^{18}\,\mathrm{cm}^{-3}$, characterized by weak PL in the IR and red (RL) region of the spectrum and a more intense PL band in the green (GL) region [1,22]. Relation of tunneling currents in the range of bias's 2.4−2.5 eV (I varies in the interval $2-10\,\mu$A) with the density of GL color centers in the *p*-GaN layer is confirmed by the temperature dependence of the GL PL intensity in the *p*-GaN layers, which increases by about two orders of magnitude upon cooling from 300 to 200 K [25], including the same temperature range as the decrease in the tunneling current (Fig. 5, curve *1*). This makes it possible to relate the decrease in tunneling leakage and, accordingly, the increase in efficiency upon cooling, to the freezing out of tunneling conduction along GL color centers due to the increase in the localization of holes at these centers. The temperature range of 200−300 K is characteristic for the unfreezing of the mobility of molecular hydrogen embedded in metals [28] or oxides [29] and for the increase in its chemical activity. This suggests the involvement of molecular hydrogen in the formation of color centers responsible for low tunneling leakage currents.

Large tunneling leakage currents in the structure B with the relatively low hole concentration ($\sim 2 \cdot 10^{17}\,\mathrm{cm}^{-3}$) in the *p*-GaN layer can be associated with the high density of RL color centers, which, according to PL data [1], is characteristic of *p*-GaN layers with insufficient activation of Mg-acceptors and a relatively high PL intensity in the red and near IR regions. The tunneling current in the region of bias's 1.65−2.2 eV (and currents $2-10\,\mu$A) corresponding to RL color centers decreases in the temperature range of 150−80 K (Fig. 5, curve *2*), in which there is an increase by two orders of magnitude of the UVL photoluminescence intensity in GaN [30] associated with donor-acceptor pairs containing hydrogen atoms. The temperature range of 80−150 K is typical for the unfreezing of the mobility of atomic hydrogen. This suggests that weakly bound atomic hydrogen is involved in the formation of RL complexes, which cause high tunneling leakage currents, an increase in which is usually observed during the degradation of GaN-based LED nanostructures.

4. Conclusion

The efficiency of localization of optically injected carriers in the InGaN/GaN quantum well is limited by the space charge of thermally and optically ionized deep centers, which increases the electric field strength near the hetero-boundaries and the tunneling permeability of the potential walls of the well, allowing the carriers tunneling from the quantum well to generate the photocurrent. With the forward bias applied to the *p*−*n*-nanostructure, the electric field strength decreases mainly in the walls of the quantum well, reducing their permeability. The decrease in the space charge at the hetero-boundaries as the impurity bands of deep color centers fill in the forward bias is reflected in the stepwise decrease in the permeability of the well walls and an increase in carrier confinement, which manifests itself as a stepwise increase in the photoluminescence intensity from the quantum well.

Conflict of interest

The authors declare that they have no conflict of interest.

References

[1] S. Nakamura, G. Fasol. The Blue Laser Diode: GaN Based Light Emitters and Lasers. Springer, Berlin, N.Y. (1998). 343 p.
[2] D. Feezell, S. Nakamura. C.R. Phys. **19**, *3*, 113 (2018).
[3] C.H. Qiu, C. Hoggatt, W. Melton, M.W. Leksono, J.I. Pankove. Appl. Phys. Lett. **66**, *20*, 2712 (1995).
[4] P. Perlin, M. Osinski, P.G. Eliseev, V.A. Smagley, J. Mu, M. Banas, P. Sartori. Appl. Phys. Lett. **69**, *12*, 1680 (1996).
[5] J.R. Lang, N.G. Young, R.M. Farrell, Y.R. Wu, J.S. Speck. Appl. Phys. Lett. **101**, 181105 (2012).
[6] H. Zhang, E.J. Miller, E.T. Yu. J. Appl. Phys. **99**, 023703 (2006).

[7] L. Esaki. In: Tunneling phenomena in solid states (Tunnel'nyye yavleniya v tverdykh telakh) / Ed. V.I. Perel'. Mir, M. (1973). P. 51. (in Russian). [Tunneling phenomena in solids / Ed. E. Burstain, S. Lundqvist. Plenium Press, N.Y. (1969)].
[8] N. Holonyak. J. Appl. Phys. **32**, *1*, 130 (1961).
[9] A.G. Chynoweth, W.L. Feldmann, R.A. Logan. Phys. Rev. **121**, *3*, 684 (1961).
[10] A.A. Klochikhin, S.A. Permogorov, A.N. Reznitsky. Physics of the Solid State **39**, **7**, 1170 (1997).
[11] S.F. Chichibu, Y. Kawakami, T. Sota. In: Introduction to Nitride Semiconductor Blue Lasers and Light Emitting Diodes / Ed. S. Naramura, S.F. Chichibu. Taylor & Francis, London–N.Y. (2000). 372 p.
[12] R.J. Molnar, T. Lei, T.D. Moustakas. Appl. Phys. Lett. **62**, *1*, 72 (1993).
[13] N.I. Bochkareva, A.M. Ivanov, A.V. Klochkov, Y.G. Shreter. J. Phys.: Conf. Ser. **1697**, 012203 (2020).
[14] M.A. Reshchikov, H.J. Morkoç. Appl. Phys. **97**, 061301 (2005).
[15] Y.T. Rebane, N.I. Bochkareva, V.E. Bougrov, D.V. Tarkhin, Y.G. Shreter, E.A. Girnov, S.I. Stepanov, W.N. Wang, P.T. Chang, P.J. Wang. Proc. SPIE **4996**, 113 (2003).
[16] L.V. Keldysh. Journal of Experimental and Theoretical Physics **33**, *4*, 994 (1957); **34**, *4*, 962 (1958).
[17] S. Nakamura, M. Senoh, N. Iwasa, S. Nagahama, T. Yamada, T. Mukai. Jpn. J. Appl. Phys. Part 2 **34**, L1332 (1995).
[18] N.G. Young, R.M. Farrell, Y.L. Hu, Y. Terao, M. Iza, S. Keller, S.P. DenBaars, S. Nakamura, J.S. Speck. Appl. Phys. Lett. **103**, 173903 (2013).
[19] N. Holonyak, Jr., D.L. Keune, R.D. Burnham, C.B. Duke. Phys. Rev. Lett. **24**, *11*, 589 (1970).
[20] N.F. Mott, E.A. Davis. Electronic processes in Non-Crystalline Materials. Clarendon Press, Oxford (1979).
[21] D. Monroe. Phys. Rev. Lett. **54**, *2*, 146 (1985).
[22] S.F. Chichibu, A. Uedono, K. Kojima, H. Ikeda, K. Fujito, S. Takashima, M. Edo, K. Ueno, S. Ishibashi. J. Appl. Phys. **123**, 161413 (2018).
[23] N.I. Bochkareva, I.A. Sheremet, Yu.G. Shreter. Semiconductors **50**, *10*, 1387 (2016).
[24] D.M. Hofmann, D. Kovalev, G. Steude, B.K. Meyer, A. Hoffmann, L. Esckey, R. Heitz, T. Detchprom, H. Amano, I. Akasaki. Phys. Rev. B **52**, 16702 (1995).
[25] M.A. Reshchikov, D.O. Demchenko, J.D. McNamara, S. Fernandes-Carrido, R. Calargo. Phys. Rev. B **90**, 035207 (2014).
[26] E. Gaubas, P. Baronas, T. Čeponis, L. Deveikis, D. Dobrovolskas, E. Kuokstis, J. Mickevičius, V. Rumbauskas, M. Bockowski, M. Iwinska, T. Sochacki. Mater. Sci. Semicon. Proc. **91**, 341 (2019).
[27] G. Yu, G. Wang, H. Ishikawa, M. Umeno, T. Soga, T. Egawa, J. Watanabe, T. Jimbo. Appl. Phys. Lett. **70**, *24*, 3209 (1997).
[28] E.G. Maximov, O.A. Pankratov. Physics-Uspekhi **116**, *3*, 385 (1975).
[29] D.L. Gricom. J. Appl. Phys. **58**, *7*, 2524 (1985).
[30] M.A. Reshchikov, R.Y. Korotkov. Phys. Rev. B **64**, 115205 (2001).